BBAA VI International Colloquium on:
Bluff Bodies Aerodynamics & Applications
Milano, Italy, July, 20–24 2008

STATIC RESPONSE COEFFICIENTS FROM DYNAMIC CABLE-MODEL TESTS

Terje L. Andersen[⋆] **and Jasna B. Jakobsen**[⋆]

[⋆]Department of Mechanical and Structural Engineering and Material Science
University of Stavanger, 4036 Stavanger, Norway
e-mails: Terje.L.Andersen@UiS.no, Jasna.B.Jakobsen@UiS.no

Keywords: Circular cable, Dry response, Static coefficients, Dynamic tests, Drag crisis.

1 INTRODUCTION

This paper summarises static response coefficients obtained from dynamic cable model tests. The response data is obtained from an elastically supported cable section model with full scale diameter. The tests were performed at the National Research Council (NRC), Canada in 2001, and have been reported in several publications, see e.g. [1]. The present paper encompasses force coefficients based on static response for all available test series. The analysis covers a total of 337 recorded time series of wind excited response. The coefficients obtained are compared to force coefficients from surface pressure data from static-model tests performed at NRC in 2002 [3, 4]. In the present abstract paper focus is on the $\phi = 60^\circ$ flow incidence situation available in both test series.

2 CABLE MODEL CHARACTERISTICS

The cable model is a spring supported steel pipe with $160mm$ HDPE cover. The springs supports are placed in two orthogonal directions perpendicular to the cable axis (*sway* and *heave*). Model inclination, ϕ, is adjustable. See table 1 for details of test setups. The cable is confined to the same vertical plane as the wind flow in all tests. However, the cable and spring supports can be rotated in order to simulate skew alignment of prototype cable and natural wind. Different levels of damping are introduced. Damping is

Case	Setup	ϕ	α	Surface	Damping
1	1B	45.0°	0.0°	smooth	low
2	1B	··	··	smooth	very high
3	1B	··	··	smooth	interm.
4	1B	··	··	smooth	high
5	1B	··	··	rough	low
6	1C	45.0°	54.7°	rough	low
7	1C	··	··	smooth	low
8	2C	60.0°	54.7°	smooth	low
9	2C	··	··	smooth	very high
10	2A	60.0°	0.0°	smooth	low
11	2A	··	··	smooth	high
12	2A	··	··	smooth	high
13	2A	··	··	smooth	vertical
14	2A	··	··	rough	vertical
15	2A	··	··	rough	low
16	3A	35.0°	0.0°	rough	low
17	3A	··	··	smooth	low
18	3B	35.0°	58.7°	smooth	low

Table 1: Parameters for test cases. *Vertical* damping denotes setups with high damping in the heave, and low damping in the sway. *Smooth* is the original clean surface condition of the HDPE material. *Rough* surface is obtained with spray-glue and contaminations of dust etc. Approx. damping relative to critical at $\sigma_{response} \approx 0.05 \cdot D$: *low*; 0.03%, *intermediate*; 0.06%, *high*; 0.24% and *very high*; 0.6% [1].

highly dependent of the response amplitude. The primary translation vibration modes of the cable model have slightly detuned natural frequencies $f_{\text{sway}} \approx f_{\text{heave}} \approx 1.4Hz$.

3 STATIC COEFFICIENTS

The dynamic time series are used to establish time averaged *static coefficients*. The raw data available is recorded deflections along spring support directions at the cable model ends. The centre point deflections in sway (s) and heave (h), perpendicular to the cable axis are determined as the mean of the corresponding end deflection, see eq. (1). In the initial position of the model (no rotation of spring supports) heave is parallel to normal component of wind flow on cable and sway is perpendicular to both wind flow and cable, see figure 1. For rotated spring supports the lift- and normal drag deflections, y and z are calculated by the transformation given in eq. (2).

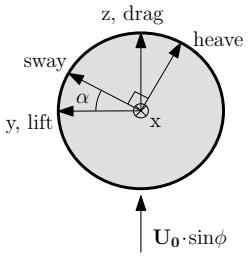

Figure 1: Cross section of cable with definition of reference coordinates and spring support rotation angle, α.

$$\begin{bmatrix} s \\ h \end{bmatrix} = \frac{1}{2} \cdot \left(\begin{bmatrix} s \\ h \end{bmatrix}_{top} + \begin{bmatrix} s \\ h \end{bmatrix}_{bottom} \right) \quad (1)$$

$$\begin{bmatrix} y \\ z \end{bmatrix} = \begin{bmatrix} \cos\alpha & -\sin\alpha \\ \sin\alpha & \cos\alpha \end{bmatrix} \cdot \begin{bmatrix} s \\ h \end{bmatrix} \quad (2)$$

$$q_0 = \frac{1}{2} \cdot \rho \cdot (U_0 \cdot \sin\phi)^2 \quad (3)$$

$$z_0 = \frac{q_0 \cdot D \cdot L}{K} \quad (4)$$

$$C_N = \frac{\overline{z}}{z_0} \ , \ C_L = \frac{\overline{y}}{z_0} \quad (5)$$

At a given tunnel wind-velocity U_0, The wind pressure normal to cable axis is defined from eq. (3). Air density is $\rho = 1.25kg/m^3$. The static reference deflection, z_0, perpendicular to cable in the cable-wind plane is established from the base pressure, cable diameter, wind exposed length of cable (here assumed to be L) and translational stiffness ($K = 31.5kN/m$) ref. eq. (4). Coefficients for the normal drag and transverse lift are then established as the ratio of time averaged deflections $\overline{y}$ and $\overline{z}$ relative to the reference deflection ref. eq. (5).The coefficients represent the total load on the cylinder. The information is thus averaged both in time and along the model dimension. The coefficients are further a measure of the combined effects of surface pressure C_{Np} and surface friction C_{Nf} [6, (1.2)]:

$$C_N = C_{Np} + C_{Nf} \quad (6)$$

For comparison to the static coefficients from dynamic tests, surface pressure data from a test series performed at the NRCC in 2002 are re-visited [4]. These tests have been discussed by Macdonald [5] in terms of the associated aerodynamic damping, relevant for development of large cable response. Figure 3b shows the normal drag coefficients derived from surface pressure tests (C_{Np}). The surface pressure recordings give information about the static coefficients C_{Np} *locally* at the circumferential ring of pressure taps (32 taps per ring).

Both dynamic- and surface pressure test series cover the critical flow transition characterised by reduction in drag (drag crisis). The ESDU correction for turbulence (λ_T), surface roughness (λ_R) and non-perpendicular incidence angle ϕ, given in eq. (7) is performed on the data [2]. Kinetic viscosity of air is $\nu = 1.5 \cdot 10^{-5} m^2/s$. In the present paper, all tested surface conditions in practice considered to be smooth and no correction is made (i.e. $\lambda_R = 1$).

$$Re_{ESDU} = \lambda_T \lambda_R \frac{U_0 D}{\nu} \cdot \frac{1}{\sin\phi} \quad (7)$$

4 DYNAMIC RESPONSE

The large dynamic responses observed during tests is the prime interest for investigation. Two types of responses are categorized as: *dry inclined cable galloping response* in case 8 and *high-speed vortex excitation* in case 10 [1]. Both incidences occurred in close proximity to the drag crisis (see figure 2a). On the subsequent figures largest responses for each case is accentuated with stars and large circles. These maximum dynamic responses can be divided into two groups: $Re_{ESDU} \approx 4.4 \cdot 10^5$ and $Re_{ESDU} \geq 5.7 \cdot 10^5$. Both Reynolds number ranges correspond to the boundary layer transition regimes TrBL1-3, according to the notation suggested by Zdravkovich [6]. On figure 2b large response is also seen to occur at non-zero lift coefficients for the majority of cases.

5 STATIC RESPONSE

The main feature of the static response is the drag crisis characterised by a sharp drop of normal drag (see figure 2 for static coefficients in all cases). The onset of drag crisis is denoted critical Reynolds number. ESDU defines critical Reynolds number for perpendicular flow drag coefficient (C_{D0}): "In general, Re_{crit} is the value of Re at which C_{D0} falls to a value of 0.8..." [2]. This suggests a $1/3$ decrease of the initial $C_{D0} = 1.2$ pre-critical plateau.

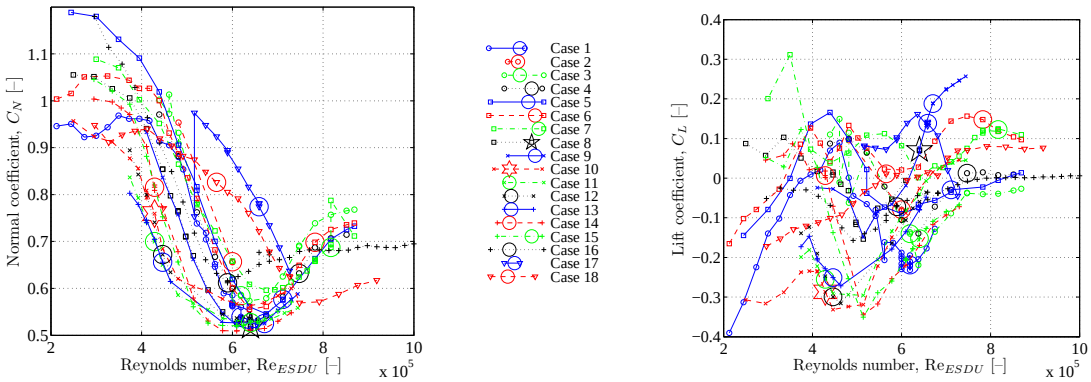

(a) Static normal drag coefficients.

(b) Static Lift coefficients.

Figure 2: Static coefficients for all dynamic cable tests.

Figure 3a shows setups with angle of incidence $\phi = 60°$. The cases include six with smooth surface and two with rough surfaces. Figure 3b shows the corresponding surface pressure coefficients for $\phi \approx 60°$. The normal drag graphs all follow quite similar paths. Assuming that a reduction to $2/3$ of drag coefficient plateau prior to drag crisis is a valid measure to define critical Reynolds number, then both test series indicate a critical Reynolds number; $\mathrm{Re}_{crit} \sim 4.0 \cdot 10^5 - 5 \cdot 10^5$. Comparing the graphs from dynamic- and surface pressure tests on figures 3a and 3b there is a systematic difference in the magnitude of the coefficients and in the post critical shape of the curves: The total normal drag coefficients from dynamic test show a pronounced local minimum of C_N after the drag crisis. C_{Np} on the other hands appears to reach a constant level immediately after the drag crisis. According to Zdravkovich, C_{Nf} in eq. (6) becomes negligible beyond shear layer transition (TrSL) at $\mathrm{Re} \approx 2 \cdot 10^5$ [6]. Based on this, a good agreement between C_N and C_{Np} could be expected in the investigated Reynolds number range. The difference in the coefficient values may thus not be affiliated with friction, but can in parts be ascribed to modelling differences between the two tests, such as tunnel blockage, end effects etc. An important difference between the two test series is the total load on full model length vs. local pressure load at specific model cross section. Zdravkovich describes a wide scatter of C_N values in the post critical *TrBL3* regime and links it to either 1) a preserved two-bubble formation similar to *TrBL2* yielding low C_N or 2) fragmentation of bubbles linked to increased C_N level [6]. The few available data points

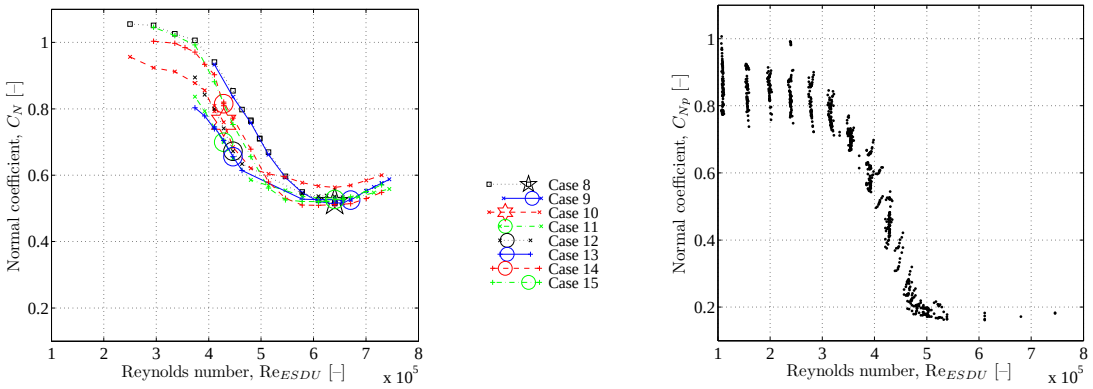

(a) Normal drag.

(b) Normal pressure drag.

Figure 3: Static coefficients for cases with angle of incidence $\phi = 60°$. (a) Dynamic test results. (b) Surface pressure results for range $\phi \in [58°; 62°]$, rings number 2 and 4 in the central part of the tested cylinder.

on figure 3b may be in any of these two bubble conditions e.g. with preserved bubbles and low C_{Np}. The length-averaged coefficients on figure 3a, can be expected to contain a combination of both bubble conditions or possibly a fully fragmented bubble state and due to this show a higher post critical drag level. The overall larger coefficients on figure 3a than those on figure 3b may indicate that the movement of the cable and resulting fluid-structure interaction contribute to overall drag.

6 CONCLUSION

Dynamic cable model response recorded for a range of influencing parameters is studied in terms of the associated static forces coefficients. Displacement time-series are translated to normal drag- and lift coefficients, as functions of effective Reynolds number. Events of large dynamic cable response described in [1] are observed to take place at the onset or the end of the drag crisis. A considerable fraction of these events appear to be associated with a non-zero mean lift coefficient. The static coefficients obtained from dynamic tests are compared to coefficients deduced from pressure surface measurements on a fixed cable model. The comparison aims at identifying and explaining discrepancies between the observed static coefficients in order to produce a wider set of available data for the investigation and better understanding of dry cable vibrations. The application of static coefficients is expected to assist in determining e.g. adequate aerodynamic damping parameter [5] or other measures to predict and suppress *divergent amplitude galloping response* and *high reduced-velocity vortex-induced-vibration* affiliated with dry circular cylinders in the vicinity of the drag crisis.

REFERENCES

[1] S. Cheng, et.al. Aerodynamic behaviour of an inclined circular cylinder. *Wind & Structures*, **6**(3):197–208, 2003.

[2] ESDU80025. *Mean forces, pressures and flow field velocities for circular cylindrical structures*. Oct. 1980.

[3] J. B. Jakobsen, G. L. Larose and M. G. Savage. *Instantaneous Wind Forces on Inclined Circular Cylinders in Critical Reynolds Number Range*. Proc. 11th Int. Conf. on Wind Engineering, Lubbock, TX, USA, June 2nd-5th, 2003.

[4] G. L. Larose, M. G. Savage and J. B. Jakobsen. *Wind tunnel experiments on an inclined and yawed circular cylinder in the critical Reynolds number range*. Proc. 11th Int. Conf. on Wind Engineering, Lubbock, TX, USA, June 2nd-5th, 2003.

[5] J. H. G. Macdonald. *Quasi-Steady Analysis of 2DOF Inclined Cable Galloping in the Critical Reynolds Number Range*. Proc. Sixth Int. Symposium on Cable Dynamics, Charleston, SC, USA, Sept. 19th-22nd, 2005.

[6] M. M. Zdravkovich. *Flow Around Circular Cylinders 1: Fundamentals*. Oxford University Press, 1997.